Supporting Information

Enhancing Charge Transfer in NiFe-LDH Anode via Ti_4O_7 Integration for High-Performance Alkaline Water Electrolysis

Qingqing Ye, [a] *Jiahao Wang,* [a] *Feifei Fang,*[b], *Yinglong Yu,*[b] *Jun Man,* [a] *Yufeng Qin,* [a] *Yanfei Wang,*[b,*] *Meiling Dou,*[a,*] *Feng Wang* [a,*]

[a] State Key Laboratory of Chemical Resource Engineering, Laboratory of Electrochemical Process and Technology for materials, Beijing University of Chemical Technology, Beijing 100029, China

[b] Petrochina Petrochemical Research Institute, Beijing, 102206, P. R. China

E-mail: wangyanfei010@petrochina.com.cn, douml@mail.buct.edu.cn, wangf@mail.buct.edu.cn

1. Experimental Section

1.1 Characterization

The crystal structures were characterized by X-ray diffraction (XRD, D8 Advance, Bruker) using Co Kα radiation. The morphological features were observed through field-emission scanning electron microscopy (FE-SEM, JSM-6701F, JEOL). The NiFe-LDH/Ti_4O_7 interface was examined using high-resolution transmission electron microscopy (HR-TEM, JSM-2100). The surface element composition and chemical states were analyzed by X-ray photoelectron spectroscopy (XPS, ESCALAB 250, Thermo Fisher), with the C 1*s* peak referenced at 284.8 eV. Raman spectroscopy (Horiba Jobin Yvon LabRam HR800) was employed to characterize the structure of samples. Nitrogen adsorption-desorption isotherms were obtained using a Quantachrome AUTOSORB-1 analyzer to evaluate the specific surface area and pore properties of samples. Fourier transform infrared spectroscopy (FTIR, Nicolet iS50) was employed to identify the surface functional groups of samples. The electrical conductivity of the samples was determined by a Hall effect instrument (RH2030, Phys Tech). The electronic band structure was analyzed using ultraviolet photoelectron spectroscopy (UPS, ESCALAB 250Xi, Thermo Fisher) and UV-vis spectrophotometry (UV-3600, Shimadzu).

1.2 Electrochemical measurements

Electrochemical measurements were conducted on a CHI760e workstation employing a standard three-electrode configuration. A glassy carbon electrode was

served as the working electrode, a graphite rod was used as the counter electrode, and a saturated calomel electrode (SCE) acted as the reference electrode. All tests were carried out in 1 M KOH electrolyte. The measured potential (E) was calibrated to the reversible hydrogen electrode (RHE) according to the following equation:

$$E(vs.\,RHE) = E(\text{vs. SCE}) + 0.241\,V + 0.0591 \times pH \qquad (Eq.1)$$

The electrocatalyst inks were prepared by dispersing 5 mg of sample in a mixture of ethanol and water (4:1 *v*/*v*) with 10 μL of Nafion solution (5 wt. %), followed by ultrasonication for at least 2 h. The electrocatalyst with the loading of 200 μg cm^{-2} was coated onto the glassy carbon electrode (0.1256 cm^2). Cyclic voltammetry (CV) was carried out within a potential window of 1.3-1.5 V versus RHE at a scan rate of 20 mV s^{-1}. Linear sweep voltammetry (LSV) was recorded over the range of 1.1-1.65 V versus RHE at 5 mV s^{-1}, with 90% iR correction applied. The Tafel slope was determined by linearly fitting the linear region of the corresponding Tafel plot in accordance with the Tafel equation:

$$\eta = a + b \times \log(j) \qquad (Eq.2)$$

In this equation, η denotes the overpotential (mV), j is the current density (mA cm^{-2}), a is a constant associated with the exchange current density, and b corresponds to the Tafel slope (mV dec^{-1}). Electrochemical impedance spectroscopy (EIS) measurements were conducted at 1.45 V versus RHE over a frequency range from 100 kHz to 0.01 Hz with a perturbation amplitude of 5 mV.

For the AWE test, NiFe-LDH/Ti_4O_7 (3 mg cm^{-2}) was served as the anode catalyst, and commercial 60% Pt/C (0.5 mg cm^{-2}) as the cathode. In a typical procedure, the

electrocatalyst powders were dispersed in ethanol by ultrasonication, followed by the addition of Nafion solution to obtain homogeneous ink. The electrocatalyst ink was spray-coated onto both side of Zirfon membrane to form the catalyst-coated membrane (CCM) electrode. The AWE performance was evaluated using a DC power supply with the cell temperature of 80 ^{o}C. Both electrodes were supplied with 30 wt.% KOH that was circulated by a peristaltic pump. Prior to measurements, the electrolyzer was activated at current densities of 100 and 500 mA cm^{-2} for 1 h each. Polarization curves were then obtained galvanostatically over a current density range of 0-2 A cm^{-2} with a stabilization time of 1 min at each current step.

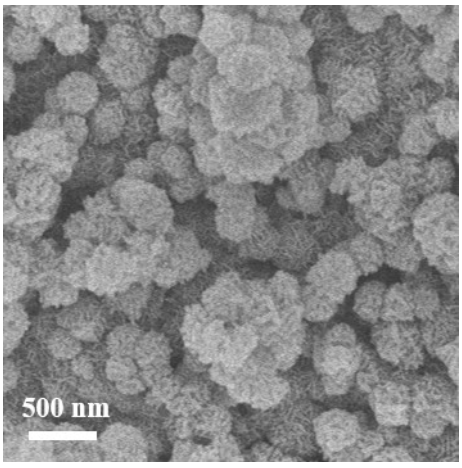

Fig. S1 SEM image of pure NiFe-LDH material.

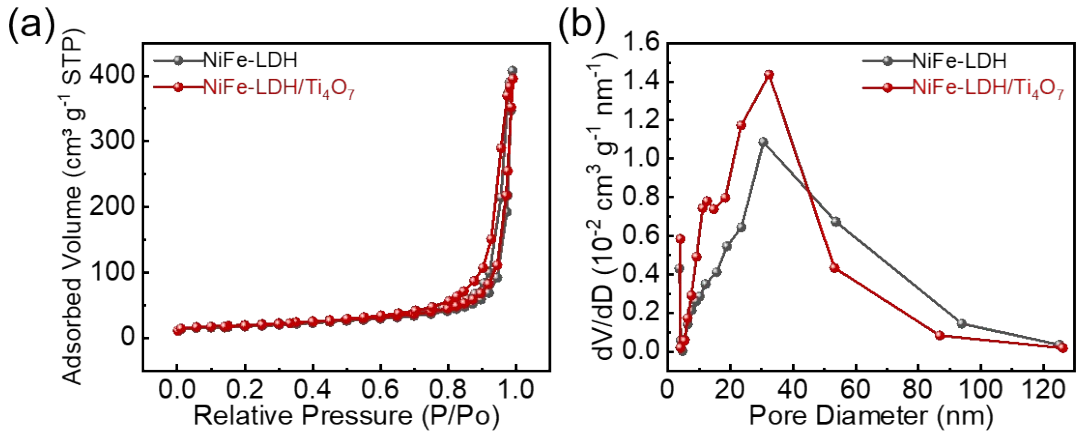

Fig. S2 (a) Nitrogen adsorption and desorption isotherms and (b) pore size distributions for NiFe-LDH and NiFe-LDH/Ti_4O_7.

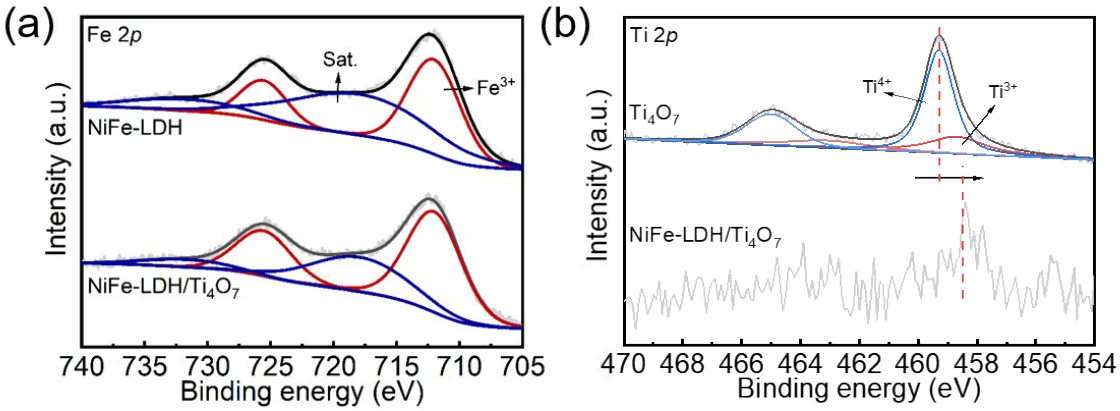

Fig. S3 High-resolution XPS spectra of (a) Fe 2*p* and (b) Ti 2*p* for NiFe-LDH/Ti_4O_7 and NiFe-LDH.

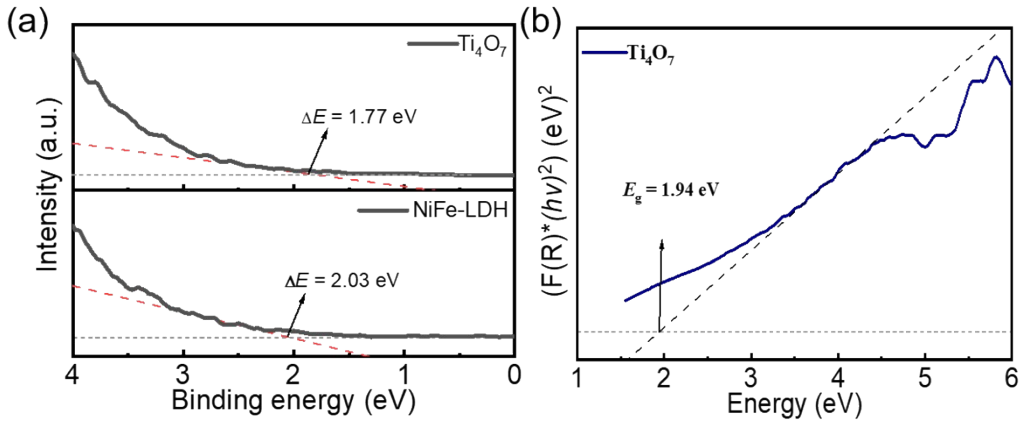

Fig. S4 (a) UPS spectra of Ti_4O_7 and NiFe-LDH. (b) Tauc plot of Ti_4O_7.

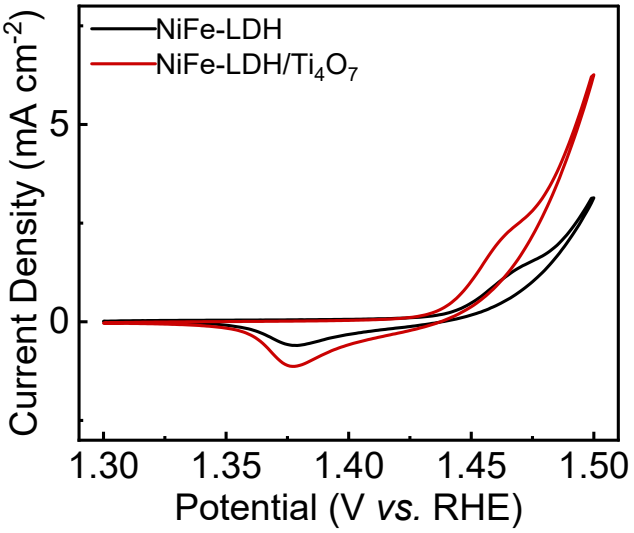

Fig. S5 CV curves of NiFe-LDH and NiFe-LDH/Ti_4O_7.

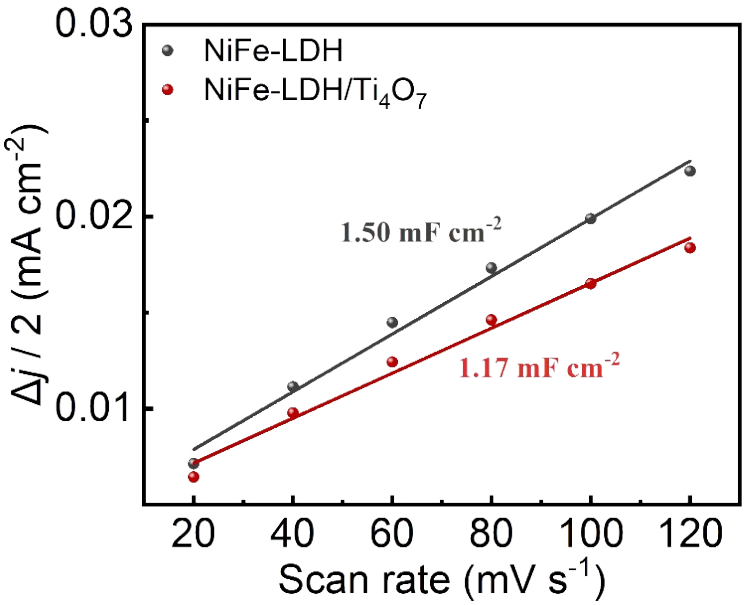

Fig. S6 Plots of current density versus scan rate.

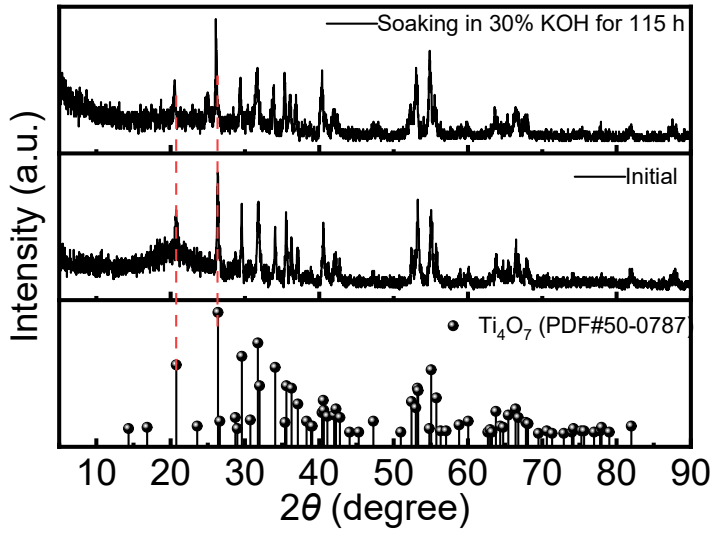

Fig. S7 XRD patterns of Ti_4O_7 before and after 115 h soaking in 30 wt.% KOH.

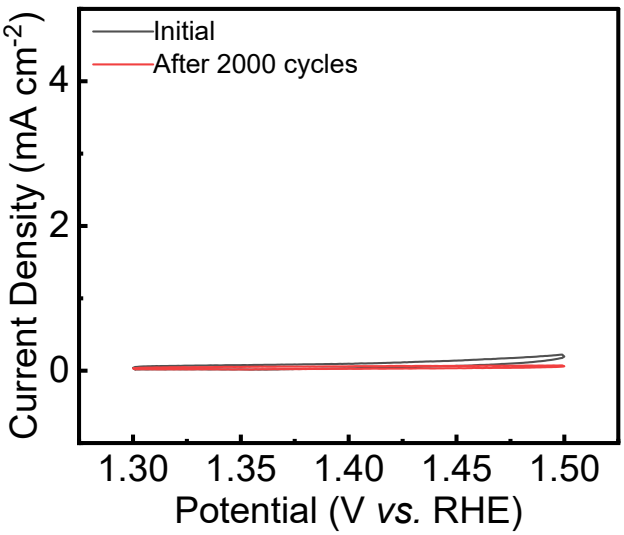

Fig. S8 Stability of Ti_4O_7 during cycling between 0.5 and 1.8 V *vs*. RHE.

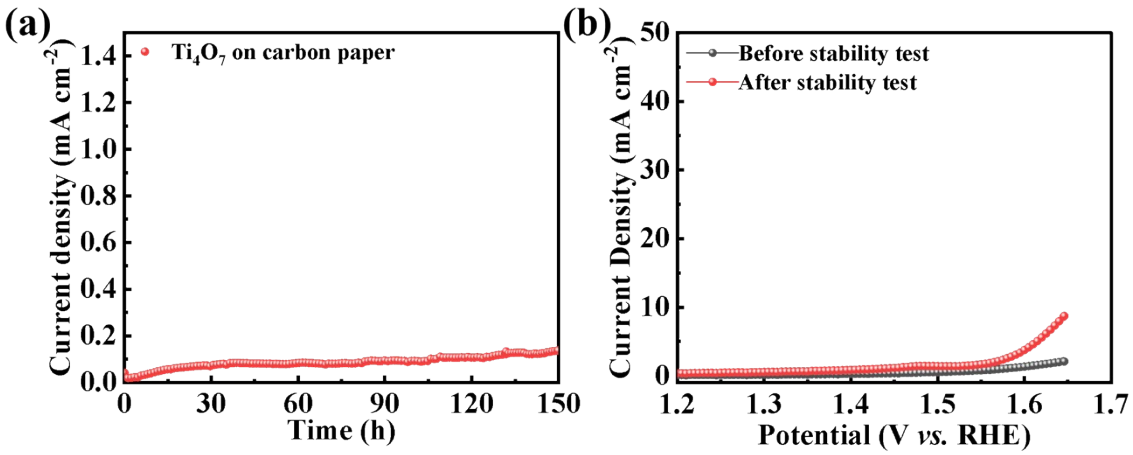

Fig. S9 (a) Stability test of Ti_4O_7 at 1.55 V *vs*. RHE in 1 M KOH and (b) LSV curves before and after stability test.

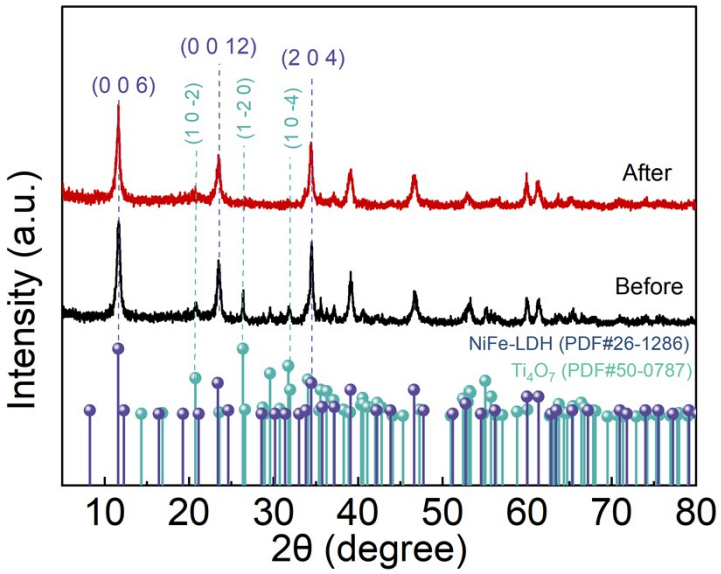

Fig. S10 XRD patterns of the NiFe-LDH/Ti_4O_7 catalyst before and after 351 h of stability test.

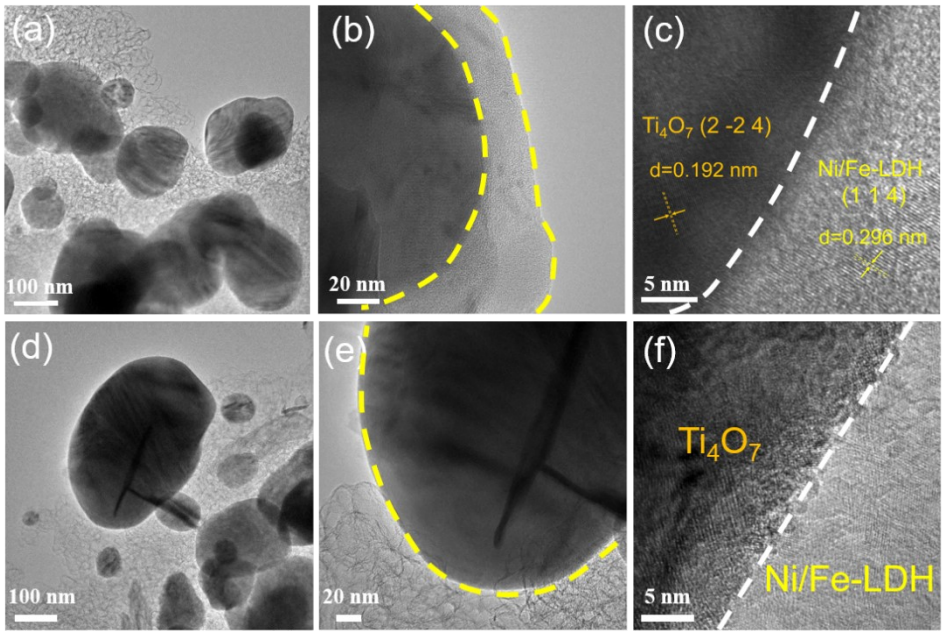

Fig. S11 HR-TEM images of the NiFe-LDH/Ti_4O_7 catalyst (a-c) before and (d-f) after 351 h of stability test.

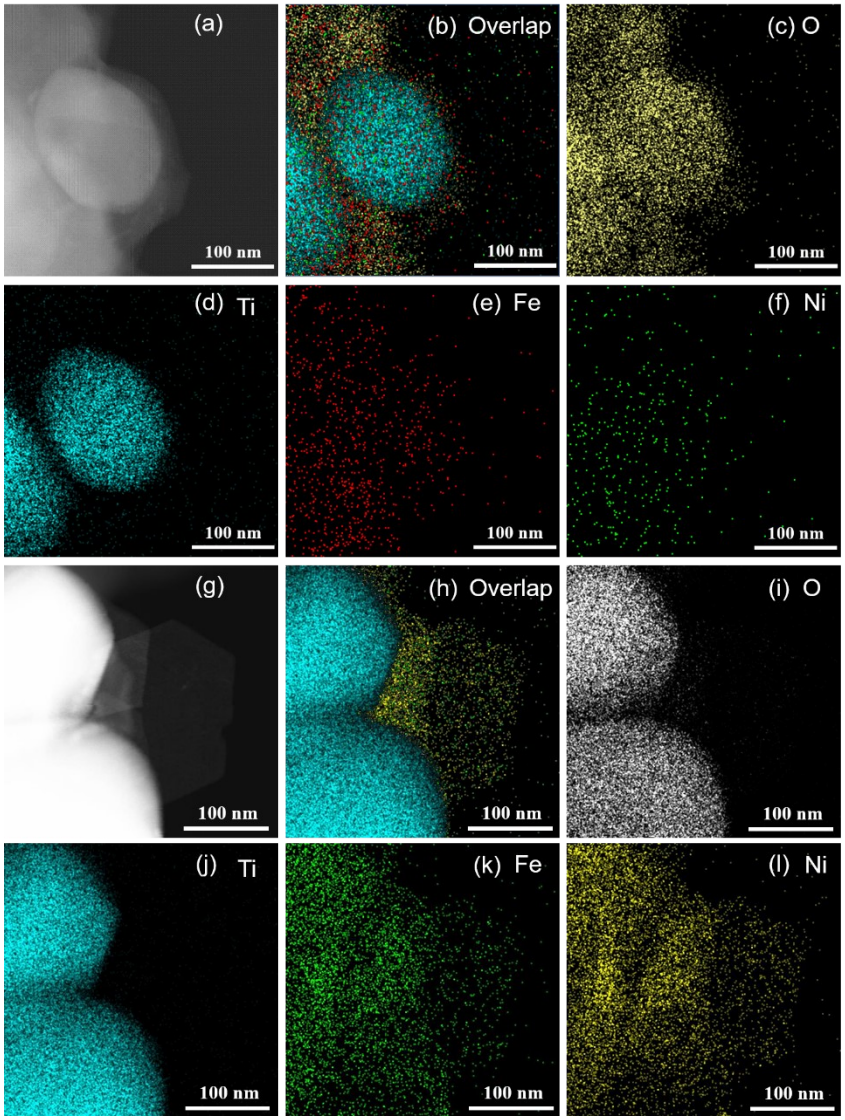

Fig. S12 Elemental mapping images of the NiFe-LDH/Ti_4O_7 catalyst (a-f) before and (g-l) after 351 h of stability test.

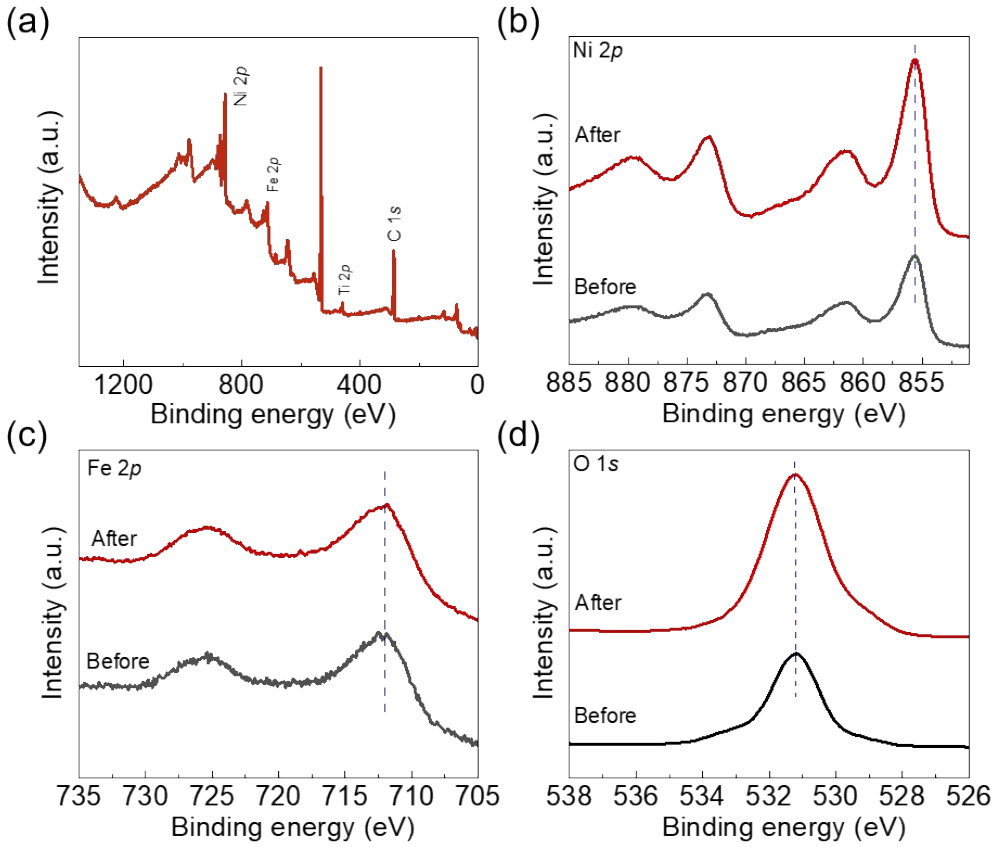

Fig. S13 (a) XPS spectrum, (b) high-resolution Ni 2*p* spectra, (c) Fe 2*p* spectra, and (d) O 1*s* spectra of NiFe-LDH/Ti_4O_7 before and after stability test.

Table S1. Comparison of performance of AWEs by using different anode materials.

Anode	Current density (mA cm^{-2})	Voltage (V)	Durability (h)	Ref.
Fe_2O_3/NiFe-LDHs	100	1.6	50	1
NiFe-TCPP	500	2.68	88	2
FePi-NiS/NF	500	2.1	30	3
$Cu_{0.81}Co_{2.19}O_4$/NF	100	1.68	100	4
NiFeCr-LDH/NF	500	1.79	40	5
NiFe//NiMo	500	1.84	50	6
S-NiFe-LDH	500	2.5	200	7
Co:NiFe-LDH@PVA	400	2.04	100	8
Mo-doped NiFe-LDH	400	1.8	24	9
NiFe-LDH/Ti_4O_7	**500**	**1.66**	**351**	**This work**

References

1. C.-F. Li, L.-J. Xie, J.-W. Zhao, L.-F. Gu, J.-Q. Wu and G.-R. Li, Applied Catalysis B: Environmental, 2022, 306, 121097.
2. Y. Hu, T. Shen, Z. Wu, Z. Song, X. Sun, S. Hu and Y.-F. Song, Advanced Functional Materials, 2025, 35, 2413533.
3. L. Guo, J. Xie, S. Chen, Z. He, Y. Liu, C. Shi, R. Gao, L. Pan, Z.-F. Huang, X. Zhang and J.-J. Zou, Applied Catalysis B: Environmental, 2024, 340, 123252.
4. W.-S. Choi, M. J. Jang, Y. S. Park, K. H. Lee, J. Y. Lee, M.-H. Seo and S. M. Choi, ACS Applied Materials & Interfaces, 2018, 10, 38663-38668.
5. T. Zhao, S. Wang, Y. Li, C. Jia, Z. Su, D. Hao, B.-j. Ni, Q. Zhang and C. Zhao, Small, 2022, 18, 2204758.
6. P. Liu, J. Wang, X. Wang, L. Liu, X. Yan, H. Wang, Q. Lu, F. Wang and Z. Ren, International Journal of Hydrogen Energy, 2024, 49, 285-294.

7. Y. Yang, W. H. Lie, R. R. Unocic, J. A. Yuwono, M. Klingenhof, T. Merzdorf, P. W. Buchheister, M. Kroschel, A. Walker, L. C. Gallington, L. Thomsen, P. V. Kumar, P. Strasser, J. A. Scott and N. M. Bedford, Advanced Materials, 2023, 35, 2305573.
8. Z. Li, G. Chen, S. Gou, X. Deng, Z. Hu and X. Lu, Journal of Alloys and Compounds, 2024, 1009, 176850.
9. A. M. Tamboli, Y. Jung, J. Sim, B. Kim, W. S. Kim, M. Kim, C. Lee, K. Kim, C. Lim, K. Kim, H.-S. Cho and C.-H. Kim, Chemosphere, 2023, 344, 140314.